

## Diffusion limited aggregation: a paradigm of disorderly cluster growth

H.E. Stanley<sup>a</sup>, A. Coniglio<sup>a,b</sup>, S. Havlin<sup>a,c</sup>, J. Lee<sup>a,1</sup>,  
S. Schwarzer<sup>a,2</sup> and M. Wolf<sup>d</sup>

<sup>a</sup> *Center for Polymer Studies and Department of Physics, Boston University,  
Boston, MA 02215, USA*

<sup>b</sup> *Dipartimento di Scienze Fisiche, Università degli Studi di Napoli, I-80125 Napoli, Italy*

<sup>c</sup> *Department of Physics, Bar-Ilan University, Ramat-Gan, Israel*

<sup>d</sup> *Institute of Theoretical Physics, University of Wrocław, ul. Cybulskiego 36,  
PL-50-205 Wrocław, Poland*

The purpose of this talk is to present a brief overview of our group's recent research into dynamic mechanisms of disorderly growth, an exciting new branch of condensed matter physics in which the methods and concepts of modern statistical mechanics are proving to be useful. Our strategy has been to focus on attempting to understand a single model system – diffusion limited aggregation (DLA). This philosophy was the guiding principle for years of research in phase transitions and critical phenomena. For example, by focusing on the Ising model, steady progress was made over a period of six decades and eventually led to understanding a wide range of critical point phenomena, since even systems for which the Ising model was not appropriate turned out to be described by variants of the Ising model (such as the *XY* and Heisenberg models). So also, we are optimistic that whatever we may learn in trying to “understand” DLA will lead to generic information helpful in understanding general aspects of dynamic mechanisms underlying disorderly growth.

### 1. Growth probabilities: simulations of DLA clusters

Like the Ising model, the rule defining DLA is simple [1]. At time 1, we place in the center of a computer screen a white pixel, and release a random walk from a large circle surrounding the white pixel. The four perimeter sites have an equal a priori probability  $p_i$  to be stepped on by the random walk. Accordingly, we write

<sup>1</sup> Present address: Levich Institute, Steinman Hall T-1M, 140th Street and Convent Avenue, New York, NY 10031, USA.

<sup>2</sup> Present address: Forschungszentrum Jülich GmbH, HLRZ, Postfach 1913, D-52425 Jülich Germany.

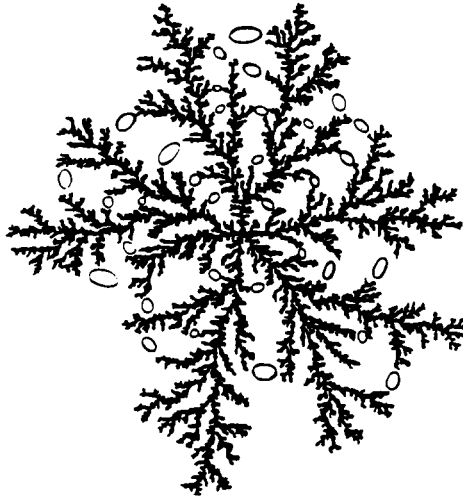


Fig. 1. Off-lattice DLA cluster of  $10^5$  sites, indicating some of the “necks” that serve to delineate “voids.” After ref. [17].

$$p_i = \frac{1}{4} \quad (i = 1, \dots, 4). \quad (1)$$

The rule is that when the random walker steps on a perimeter site, it sticks irreversibly. This forms a cluster of mass  $M = 2$ , with  $N_p = 6$  perimeter sites, henceforth called *growth sites*. Now the probabilities are *not* all identical: each of the growth sites of the two tips has growth probability  $p_{\max} \cong 0.22$ , while each of the four growth sites on the sides has growth probability  $p_{\min} \cong 0.14$ .

Just because the third particle is *more likely* to stick at the tip does not mean that the next particle *will* stick on the tip. Indeed, the most that one can say about the cluster is to specify the *growth site probability distribution* (GSPD), i.e., the set of numbers,

$$\{p_i\}, \quad i = 1, \dots, N_p, \quad (2)$$

where  $p_i$  is the probability that perimeter site (“growth site”)  $i$  is the next to grow, and  $N_p$  is the total number of perimeter sites ( $N_p = 4, 6$  for the cases  $M = 1, 2$ ). The recognition that the set of  $\{p_i\}$  gives us essentially the *maximum* amount of information we can have about the system is connected to the fact that tremendous attention has been paid to these  $p_i$ .

If the DLA growth rule is iterated  $10^5$  times, then we obtain a large cluster (fig. 1) characterized by a range of growth probabilities that spans several orders of magnitude – from the tips to the fjords – so that histograms of these growth probabilities typically use a logarithmic scale for the abscissa (fig. 2).

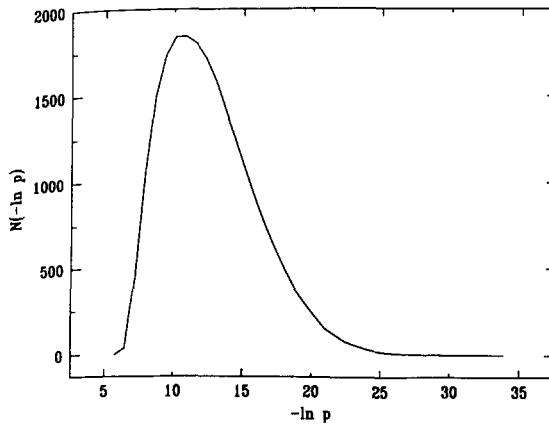


Fig. 2. The histogram  $N(-\ln p)$  for 3D DLA. The quantity  $N(-\ln p) d \ln p$  is the average number of growth sites with growth probabilities  $p'$  such that  $-\ln p < -\ln p' < -\ln p + d \ln p$ . Here, we display data for 50 off-lattice clusters of mass 15 015.

Diffusion limited aggregation (DLA) has become important for describing a wealth of diverse physical and chemical phenomena [2]. Recently, several phenomena of *biological* interest have also attracted the attention of DLA aficionados. These include the growth of bacterial colonies [3], the retinal vasculature [4], and neuronal outgrowth [5]. The last example is particularly intriguing since if evolution chose DLA as the morphology for the nerve cell, then perhaps we can understand “why” this choice was made. What evolutionary advantage does a DLA morphology convey? Can we use the answer to this question to better design the next generation of computers? Already we appreciate that a fractal object is the most efficient way to obtain a great deal of intercell “connectivity” with a minimum of “cell volume,” so one immediate question is “which” fractal did evolution select, and why?

We will save time and space by resisting the temptation at this point to “pull out the family photo album” to show lots of realizations. Instead, we may refer the interested reader (and their non-specialist colleagues) to the album ‘Les Formes Fractales’ (and its English translation ‘Fractal Forms’) prepared in connection with a hands-on exhibition of the same name that is currently on view at the Palais de la Découverte in Paris [6].

As with many models in statistical mechanics, the theoretical challenge is as important as the experimental realizations in “hooking” theorists. And as with many statistical mechanical models, the defining rule in DLA is simple even though the consequences of that rule are extremely rich. Understanding how such a rich consequence can follow from such a simple rule is indeed an irresistible challenge.

In the case of DLA, this challenge is enhanced by the fact that – unlike other models with simple rules (such as the Ising model) – in DLA there is no Boltzmann factor so we can more easily explain and understand since one does not have to know any physics beforehand. Indeed, it initially surprises almost everyone who sees DLA develop in real time on a computer screen that a complex outcome (at the *global* level of a “form”) seems to bear no obvious relation to the details of the simple rule that produced this form – at least, I have known no one who predicted exactly the “form” of DLA from knowledge only of the rule.

Despite remarkable recent progress [7–14], no genuine understanding of DLA has emerged. There have been attempts to measure and understand the distribution of  $p_i$ , and its lower cutoff  $p_{\min}$ , as well as to understand the the discovery of a “phase transition” in the behavior of the moments of the distribution, and the connection between multifractality and multiscaling [8–14]. However, the issue is still far from being settled.

For example, the mass dependence of  $p_{\min}$  is important in establishing the nature of the phase transition. There are suggestions of exponential [10],

$$p_{\min} \sim \exp(-AM^x), \quad (3)$$

power law [11]

$$p_{\min}(L) \sim M^{-\alpha}, \quad (4)$$

and an “intermediate” behavior [12]

$$p_{\min}(L) \sim M^{-\log M} \quad (\log p_{\min} \sim -(\log M)^2). \quad (5)$$

Each of these forms can be related to a possible fjord structure:

- (a) The exponential form [10] corresponds to narrow necks (of length  $M^\beta$  with  $\beta > 0$ ).
- (b) The power law form [11] corresponds to wedge type fjords.
- (c) The “intermediate” behavior [12] can be explained in terms of a structural model of DLA, which has self-similar *voids* connected by *necks*, as explained in the next section [12,13].

The scaling form of the complete growth site probability distribution  $\{p_i\}$  is also of interest. Trunfio and Alstrøm [10], Mandelbrot and Evertsz [10] and Schwarzer et al [12] proposed different types of possible behavior.

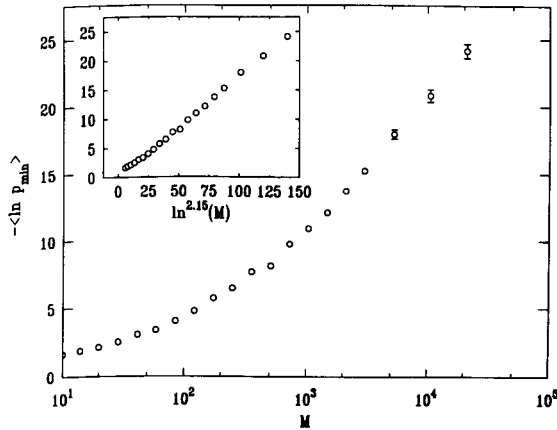


Fig. 3. Quenched average  $-\langle \ln p_{\min} \rangle$  of the minimum growth probability  $p_{\min}$  in 19 2D off-lattice DLA clusters as a function of the cluster mass  $M$ , where  $10 < M < 21\,000$ . Note the upward curvature in the log-log representation, which indicates that  $p_{\min}$  decays faster than any power-law as function of  $M$ . The inset shows the same quantity, but plotted vs  $(\ln M)^{2.15}$ ;  $p_{\min}$  displays straight-line behavior from  $M \simeq 90$  up to the maximum  $M = 21\,000$ , so the functional dependence of  $p_{\min}$  on  $M$  can be written as  $\ln p_{\min} \sim \ln^{2.15} M$ . The error on the exponent 2.15 is about  $\pm 0.2$ .

## 2. The “void-neck” model of DLA structure

Our own group’s numerical results (e.g., fig. 3) support possibility (c), and may provide a clue for the underlying puzzle of understanding DLA structure [12]. Specifically, we have proposed a “void-neck” model of DLA [12] in order to explain the result (5). The void-neck model states that each fjord is characterized by a hierarchy of voids separated from each other by narrow “necks” or “gateways.” The key feature of the model are (i) the distribution of voids must be *self-similar*, and (ii) the voids are separated by necks (“channels,” or “gateways”); a random walker can pass from one void to the next only by passing through a gateway.

What is the evidence supporting the void-neck model of DLA growth dynamics?

- (1) First, we note that if necks “dominate”, then (3) would have to be satisfied. The numerics rule this out.
- (2) Second, we note that if self-similar voids dominate, then (4) would have to be satisfied. Again, the numerics rule this out.
- (3) Photos of large DLA clusters reveal the presence of such voids and necks (fig. 1). Moreover, when the DLA mass is doubled, we find that outer branches “grow together” to form new necks (enclosing larger and larger voids).

- (4) The void-neck model can be *solved* under the approximation that the voids are strictly self-similar and the gates are narrow. The solution demonstrates that  $\log p_{\min} \propto (\log M)^2$ .
- (5) The void-neck model is consistent with a recent calculation [14] suggesting that DLA structures can be partitioned into two zones:
- (a) An inner *finished zone*, typically with  $r \leq R_g$  (where  $R_g$  is the radius of gyration), for which the growth is essentially “finished” in the sense that it is overwhelmingly improbable that future growth will take place.
  - (b) An outer *unfinished zone* (typically  $r \geq R_g$ ) in which the growth is unfinished.

Thus future growth will almost certainly take place in the region  $r > R_g$ . Now  $2R_g \approx \frac{1}{2}L$ , where  $L$  is the spanning diameter. Hence only about  $\frac{1}{4}$  the total “projected area” of DLA is finished, the rest of the DLA being *unfinished*. We suggest that the finished region will be created from the unfinished region by tips in the unfinished region growing into juxtaposition (thereby forming voids). The growth of DLA is fixed by the growth probabilities, which are of course largest on the tips.

Indeed, two tips will grow closer and closer until their growth probabilities become so small that no further narrowing will occur. This observed phenomenon can be perhaps better understood if one notes that the growth probabilities  $\{p_i\}$  of a given DLA cluster are identical to normalized values of the electric field  $\{E_i\}$  on the surface of a charged conductor whose shape is identical to the given DLA cluster. Thus as two arms of the DLA “conductor” grow closer to each other, the electric field at their surface must become smaller (since  $E_i \propto \nabla\phi_i$ , where  $\phi \equiv$  constant on the surface of the conductor). That  $E_i$  is smaller for two arms that are close together can be graphically demonstrated by stretching a drumhead with a pair of open scissors.

- (1) If the opening is big, the tips of the scissors are well-separated and the field on the surface is big (we see that the gradient of the altitude of the drumhead is large between the tips of the scissors).
- (2) On the other hand, if the scissor tips are close together, the field is small (we see that the gradient of the altitude of the drumhead is small between the scissor tips).

### 3. Exactly-solvable deterministic model of DLA

Lee et al. [13] developed a hierarchy of deterministic fractal models designed to capture some of the essentials in the structure of DLA. These models, whose key ingredients are narrow necks and self-similar voids, are gener-

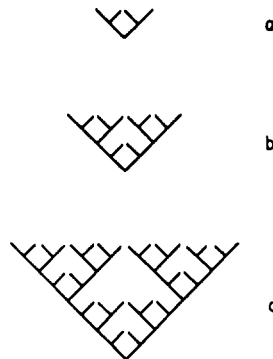


Fig. 4. Construction of a deterministic hierarchical model for DLA. (a) The generator and the first generation of the model; (b) the second generation; and (c) the third generation. After ref. [13].

alizations of the model presented in refs. [12,13]. *We find an analytic solution of the growth site probability distributions for the entire family of models.* This distribution is found to have the same form as that of DLA clusters recently measured by Schwarzer et al. [12],  $n(\alpha, M) \sim \exp[-A\alpha^\gamma (\ln M)^{-\delta}]$ , where  $n(\alpha, M) d\alpha$  is the number of growth sites with  $\alpha < -\ln p_i / \ln M < \alpha + d\alpha$ . The two exponents ( $\gamma = 2 \pm 0.3$ ,  $\delta = 1.3 \pm 0.3$ ) found numerically by Schwarzer et al. [12] to characterize the distribution, are found analytically by Lee et al. [13] to be 2 and 1, respectively. It is possible that the form of the distribution and the exponents are determined *only* by the presence of the necks and self-similar voids, independent of further details of models. The agreement between the distribution (and its exponents) of DLA and the models provides further support for the void-neck description of the structure of DLA.

The model is defined as follows. The first generation (fig. 4a), consists of three wedges, is the generator of the model. In order to get the next generation, we replace every wedge in the first generation with the generator (fig. 4b). The third generation is obtained by replacing every wedge in the second generation with the generator (fig. 4c). In general, one can obtain generation  $n$  by replacing all the wedges of the generation  $n - 1$  with the generator.

In order to obtain the growth site probability distribution  $n(\alpha, M)$ , Lee et al. [13] expand the distribution, using the Cauchy identity, in terms of Gauss polynomials. Each distribution for one Gauss polynomial “marginally” overlaps with all the other terms. This fact permits the re-summation of the expansion to get a closed form for  $n(\alpha, M)$ . Due to the “marginal” overlap, one cannot obtain the exact amplitudes for the distribution, but we find approximate values, which are in good agreement with exact numerical data.

One interesting point to emerge is that the distribution is the same (except amplitudes) for the entire family of models studied in ref. [13]. Since the common ingredient for the entire family is a hierarchy of self-similar “voids” separated by narrow necks, it is possible that the form of  $n(\alpha, M)$  obtained here is just a consequence of the void-neck feature, and is independent of further details of a model.

#### 4. Scaling properties of the perimeter of DLA: the “glove” algorithm

Almost all the sites of a fractal lie on its surface. This simple observation explains why fractals are of great importance in a wide range of disciplines. In biology, matter exchange takes place across membranes and often requires large contact areas of the participating systems: oxygen diffuses into the blood in lung tissue and trees absorb nutrients through their widely branched root network. In chemistry, reaction rates depend on the surface that the reacting species expose to each other; the surface of a catalyst plays a central role in catalytically controlled reactions; important for applications is also the use of porous media as electrodes for batteries.

Very recently, Schwarzer et al. [15] introduced a “glove” algorithm and used it to carry out a systematic study of various properties of the DLA and percolation perimeters. They developed an algorithm – the “glove” method – which can be applied to study topological properties of any fractal (or self-affine) surface. In particular, the glove method can be used to determine:

- (i) the total perimeter of a fractal, the set of all nearest neighbor sites of the fractal, and a generalization thereof to neighboring sites of higher order – here Schwarzer et al. find a scaling relation which also suggests a novel method for the determination of the fractal dimension of an object;
- (ii) the accessible perimeter of a fractal, which is the set of the perimeter sites that can be reached from the exterior of the object, and a generalization thereof to neighbor sites of higher order – this quantity has been studied experimentally on porous media and fresh fractures, and theoretically on percolation clusters.
- (iii) the “lagoon”-size distribution, where “lagoons” are generalizations of the notion of voids to the case of *loopless* fractals and describe the regions of a fractal inaccessible to probes with a given particle size. The glove algorithm also enables one to identify unambiguously “necks” in a fractal structure.

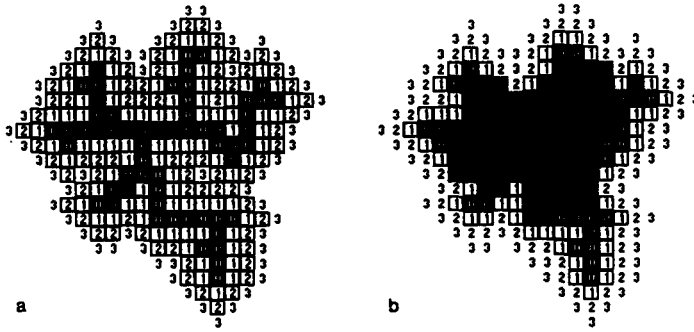


Fig. 5. (a) To illustrate the construction of the  $\ell$ -perimeter we show the object and the  $\ell$ -perimeters with  $1 \leq \ell \leq 3$ . Sites belonging to the investigated object are displayed in black and bear the label 0. Other numbers denote the order of the  $\ell$ -perimeter. (b) Lagoons are constructed by placing flexible gloves, one lattice unit thick, on the object. The gloves cannot penetrate through narrow openings. In our example, the 2-glove has “sealed” all openings, and we identify the enclosed space as lagoons (grey sites). After ref. [15].

#### 4.1. Determination of the $\ell$ -perimeter

We begin by representing the investigated object in discretized form on a lattice and label its sites with the index 0 (black sites in fig. 5). In the first step, we find all the nearest-neighbor sites of the object and label them  $\ell = 1$ , as shown in fig. 5a. Those sites that are nearest neighbors of sites with  $\ell = 1$  and not already labeled are identified as  $\ell = 2$  sites. We repeat the procedure and obtain  $\ell$  values for all sites surrounding the object (see fig. 6). The number  $\ell$  associated with every lattice site is called the topological distance of the site to the object. We will use the term “ $\ell$ -perimeter” to refer to the set of sites with label  $\ell$ . Schwarzer et al. [15] argued that  $\Pi(M, \ell)$ , the number of sites of the  $\ell$ -perimeter, should obey a scaling law of the form  $\Pi(M, \ell)/\ell \sim f(\ell/M^{1/d_f})$ , where  $f(u) \sim u^{-d_f}$  for  $u \rightarrow 0$  and  $f(u) \rightarrow \text{const.}$  for  $u \rightarrow \infty$ . Simulations of 21 2D off-lattice DLA clusters (and also 50 2D percolation hulls) support this relation.

#### 4.2. The $\ell$ -gloves

Next we describe the procedure to determine the “ $\ell$ -gloves” of the object. In the first step, instead of labeling all the neighbor sites, we place a flexible “glove,” one lattice unit thick, on the object. In general, since gloves cannot penetrate through the narrowest openings (less or equal to  $\sqrt{2}$  lattice constants wide), they cannot cover the object completely. The second glove is placed on the union of object and 1-glove. We iterate the covering process to obtain

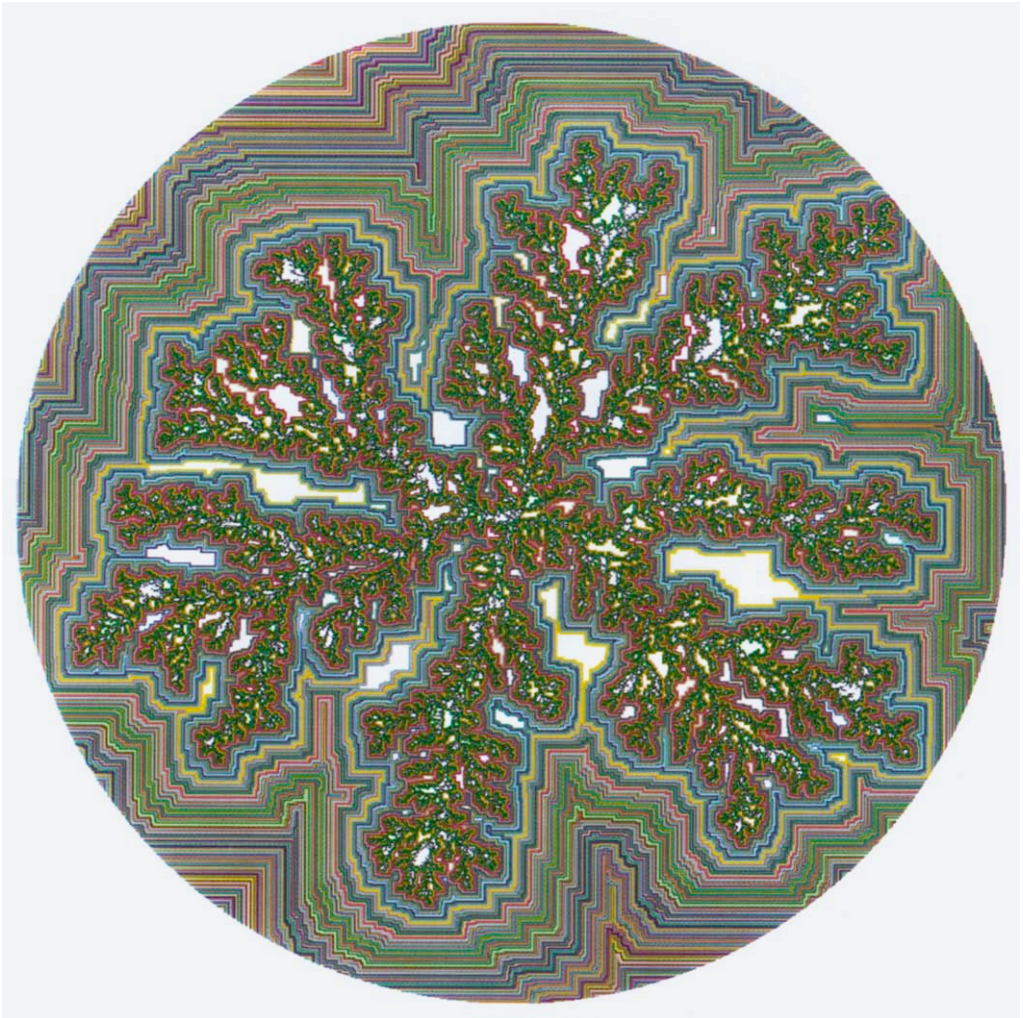


Fig. 6. Large off-lattice DLA cluster with 50 000 sites, covered by a series of successive gloves ( $\ell = 1, 2, 3, \dots$ ).

$\ell$ -gloves up to any desired order. Fig. 5b illustrates the glove algorithm by showing the gloves of order  $\ell = 1, 2, 3$  for a small DLA cluster. Note that the 1-glove penetrates the “fjords” of the object but the 2-glove cannot. Unlike the  $\ell$ -perimeter, the  $\ell$ -glove comprises only those sites that can be reached from the exterior without stepping on any other site of the  $\ell$ -perimeter, and so forms a connected subset of the  $\ell$ -perimeter. Like the  $\ell$ -perimeter, the subsequent gloves explore fewer and fewer details of the surface of the object. The  $\ell$ -perimeter and the  $\ell$ -glove are identical for large  $\ell$  (greater than the “radius”

of the largest “lagoon”, see below).

### 4.3. Necks and lagoons

Significantly, the glove algorithm can be used to extend to the case of loopless fractals the notion of voids as empty spaces in multiply connected fractals. Imagine, e.g., a circle with a small opening of width  $w = 2\ell_o$ , a simple example of a loopless object. Cover the surface with gloves, one after the other. When the number of gloves reaches  $\ell_o$ , the glove cannot penetrate into the opening. We denote by “lagoon” the set of points left in the interior – now inaccessible from the exterior. The number of enclosed sites is the lagoon size  $s$ . The sites, where glove  $\ell_o$  touches itself, identify a “neck.” Note that there exists a one-to-one correspondence of lagoons and necks, so that each lagoon has a unique neck width  $w$  given by  $w = 2\ell_o$ . For the object in fig. 5b, all the necks of lagoons have width  $w = 4$ . Schwarzer et al. [15] found that the lagoon size distribution in DLA is consistent with a self-similar structure of the aggregate, but that even for large lagoons the most probable width of the necks that separate the lagoons from the exterior is very small.

## 5. Multifractal scaling of 3D DLA

In a recent work [16], the multifractal spectrum of the growth probability of 3D off-lattice DLA was studied. The results indicate that, in contrast to 2D DLA, there appears to be *no* phase transition in the multifractal spectrum. Why? In both 2D and 3D, “necks” are created by side branches in DLA that grow closer and closer until their growth probabilities become so small that no further narrowing occurs. However, in 3D, even if there are points where tips from different branches of the aggregate come close or meet, there is no significant screening of growth due to this configuration, because no volume is cut off from the exterior and particles can enter the cluster from a direction perpendicular to the loop. Simply stated, one cannot cut off a volume with branches in the same way one can cut off an area. Thus we interpret the apparent absence of a phase transition for 3D as the effect of the topological differences between 2 and 3 dimensions. We further note that as  $d$  increases,  $d_f$  becomes closer to  $d - 1$ ; the higher  $d$  is, the less dense the clusters are, since  $\rho(R) \sim R^{d_f-d}$ . Thus it is tempting to conjecture that  $d = 2$  is a “lower critical dimension” in the sense that there is a phase transition for  $d = 2$  but power-law scaling for all  $d > 2$ .

In sum, for 3D, even when tips from different branches are close, there is no significant screening of growth, since particles can enter from directions

perpendicular to the loop, suggesting a power-law dependence of  $p_{\min}$  on the mass  $M$  of the cluster. Thus the apparent absence of a phase transition in 3D DLA can be interpreted as due to the topological difference between 2 and 3 dimensions. We have calculated the  $\{p_i\}$  for 50 off-lattice 3D DLA clusters, and compared our analysis to the 2D case which is believed to undergo a phase transition. We find the 3D case is quite different. Specifically, we find

- (i) the local slopes  $\tau(q, M) \equiv \partial \ln Z / \partial \ln M$  do not diverge for  $q < 0$  as they do in 2D (here  $Z$  denotes the  $q$ th moment of the distribution  $\{p_i\}$ ),
- (ii) The Legendre transform function  $f_L(\alpha) \equiv q\alpha - \tau$  (where  $\alpha \equiv \partial \tau / \partial q$ ) has no systematic mass dependence, as it has in 2D, and
- (iii)  $p_{\min}$  has a power-law singularity in  $M$ , following eq. (4), in contrast to the 2D case, where  $p_{\min}$  vanishes much faster, according to (5).

### 6. Multiscaling

However complex the above picture of DLA may seem already, there are even richer scaling features in this growth paradigm: DLA also exhibits *multiscaling*.

To see what this means, let us first introduce the annular mass  $\rho_A(x, M)$ , where  $\rho_A(x, M) dx$  is the number of sites in the annulus  $[x, x + dx]$  in a cluster of mass  $M$ . We define  $x_i \equiv r_i/R$  as the distance of a cluster site  $i$  from the seed, normalized by the radius of gyration  $R$  of the cluster (see figs. 7,8). The conventional mass density  $\rho(r)$  is related to  $\rho_A(x, M)$  by  $\rho_A(x, M) dx = 2\pi r \rho(r, M) dr$ . Let us next introduce the set of fractal dimensions  $D(x)$  characterizing the mass distribution within each annulus  $x$ . In conventional scaling,  $D(x) = d_f$  is independent of  $x$ . In DLA, however, calculations suggest that  $D(x)$  depends on  $x$ . Such calculations also support the following *multiscaling ansatz* [14],

$$\rho_A(x, M) \sim r^{D(x)} C(x), \tag{6}$$

where  $C(x)$  is a “cut-off function” to ensure that  $\rho_A = 0$  outside the cluster. The connection to the usual fractal dimension is that  $d_f$ , the fractal dimension of the entire cluster, is equal to the maximum of  $D(x)$ , since asymptotically only sites in the annuli with  $D(x) = d_f$  contribute to the total mass of the cluster.

To gain insight into the conditions under which multiscaling arises, consider the joint distribution function  $N(\alpha, x, M)$ , where  $N(\alpha, x, M) d\alpha dx$  is the number of growth sites in the annulus  $[x, x + dx]$  and with  $\alpha$  values in the interval  $[\alpha, \alpha + d\alpha]$ . The distribution  $N(\alpha, x, M)$  contains all the information



Fig. 7. A DLA configuration with the shaded region corresponding to a shell characterized by a value  $x \equiv r/R$ .

of  $n(\alpha, M)$ , since  $n(\alpha, M)$  (cf. section 2) can be recovered by integration of  $N(\alpha, x, M)$  with respect to  $x$ ,

$$n(\alpha, M) \equiv \frac{\int dx N(\alpha, x, M)}{\int dx d\alpha N(\alpha, x, M)}. \quad (7)$$

However,  $N(\alpha, x, M)$  provides additional information about the location of growth sites with a specific  $\alpha$  value which is not contained in  $n(\alpha, M)$ . A reasonable approximation to  $N(\alpha, x, M)$  is a Gaussian in  $x$ , namely

$$N(\alpha, x, M) = \frac{M^{f(\alpha)}}{\sqrt{2\pi\xi^2(\alpha, M)}} \exp\left(-\frac{[x - \bar{x}(\alpha, M)]^2}{2\xi^2(\alpha, M)}\right), \quad (8)$$

with mean square width  $\xi^2(\alpha, M)$  and center  $\bar{x}(\alpha, M)$ . The function  $\bar{x}(\alpha, M)$  appears to converge for large  $M$  to a limit  $\bar{x}(\alpha)$  [14].

Since the growth sites of DLA are associated with cluster sites, we expect that  $\rho_A(x, M)$  is proportional to the density profile of growth sites, which follows from (8) by integration over  $\alpha$ , i.e.,

$$\rho_A(x, M) \sim \int d\alpha N(\alpha, x, M). \quad (9)$$

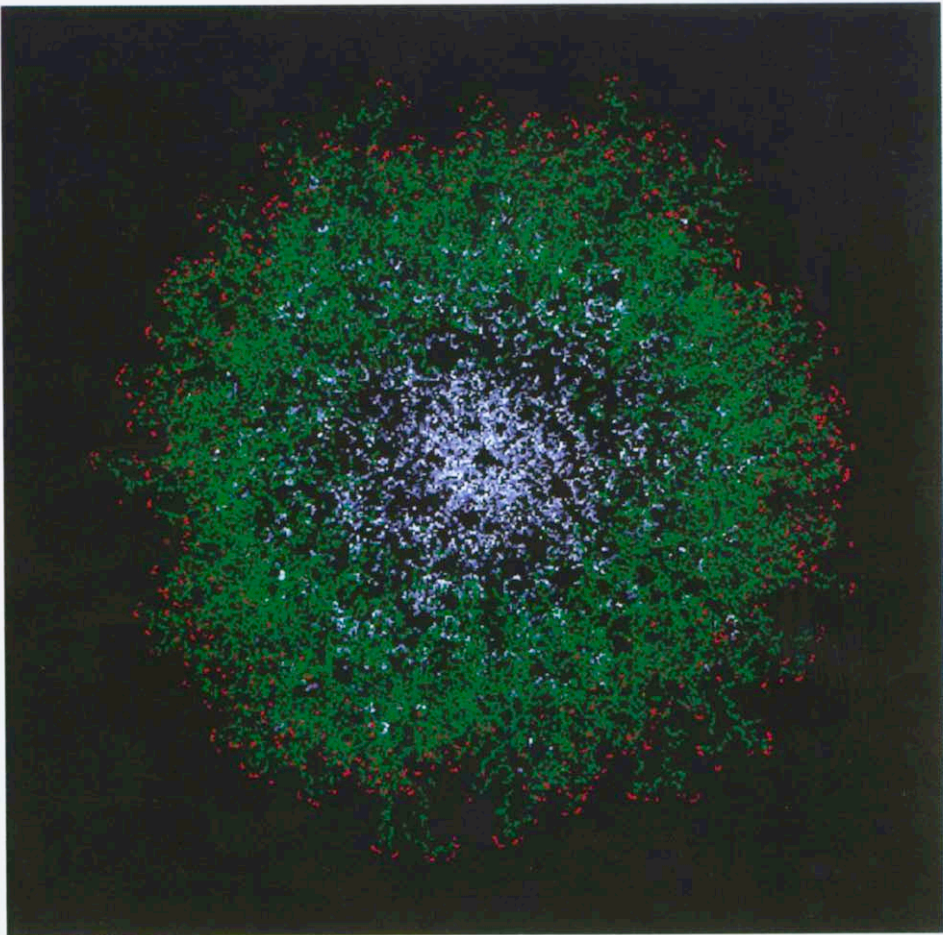


Fig. 8. Nineteen superposed 2D off-lattice DLA clusters. Three subsets of the growth sites are colored according to their  $\alpha$  values. Red denotes the range  $0.4 < \alpha < 0.8$ , green  $0.8 < \alpha < 1.2$ , white  $3.8 < \alpha < 4.2$ . Note that large  $\alpha$  values correspond to sites with small growth probabilities. We see that growth sites with specific values of  $\alpha$  are located in approximate annuli characterized by different average positions  $\bar{x}(\alpha, M)$  (where  $x \equiv r/R$ ) and different widths  $\xi(\alpha, M)$ .

There are three distinct possibilities for the functional dependence of the width  $\xi(\alpha, M)$ . We discuss these and their implications next.

*Case (i): "constant width"  $\xi(\alpha, M) = A(\alpha)$*

A constant width corresponds to having both the average location  $\bar{x}(\alpha)$  of the  $\alpha$ -sites and the width of the growth zone not mass dependent. This implies that both length scales are proportional to the cluster radius  $R$ . Substituting (8) into (9) and performing a steepest descent of the resulting integral, leads

to the cluster density profile

$$\rho_A(x, M) \sim r^{d_f} C(x). \quad (10)$$

Since the exponent  $d_f$  is the fractal dimension of the cluster, in case (i) conventional scaling arises.

*Case (ii): "strong localization"  $\xi(\alpha, M) = A(\alpha) M^{-\gamma}$*

In this case a similar analysis to that of case (i) reveals that the annular density displays multiscaling,

$$\rho_A(x, M) \sim r^{f(\alpha^*(x))} C(x), \quad (11)$$

where  $\alpha^*(x)$  is the inverse function of  $\bar{x}(\alpha)$  and  $f$  is from eq. (8). The form in (11) is not altogether surprising. Because in this case the width of the distribution  $N(\alpha, x, M)$  for fixed  $\alpha$  tends to zero as  $M \rightarrow \infty$ , in this limit almost all the sites with a specific  $\alpha$ -value are located at distance  $\bar{x}(\alpha)$  from the cluster seed. That is why we refer to case (ii) as "strong localization." Conversely, a specific location  $x$  singles out an  $\alpha$  value  $\alpha^*(x)$ . From  $f(\alpha)$  we then obtain the fractal dimension of the set of these  $\alpha^*(x)$ -sites. Eq. (11) can now be understood as the conventional relationship between mass and extension of a fractal object.

*Case (iii): "weak localization"  $\xi(\alpha, M) = A(\alpha)/(\ln M)^{1/2}$*

The logarithmic factor in  $\xi(x, M)$  in case (iii) changes the exponential term of eq. (8) into a power law, which gives rise to qualitatively new scaling phenomena. As in case (ii), the exponent  $D(x)$  is  $x$ -dependent so that multiscaling arises [14]. While in case (ii) only the typical  $\alpha$ -values (namely those for which the average location  $\bar{x}(\alpha) = x$ ) enter  $D(x)$ , in case (iii) we observe contributions from other  $\alpha$  values. Thus, we refer to case (iii) as a case of "weak localization." There is still some localization since the width is still vanishing with increasing mass.

Thus, like the distribution of growth probabilities, the adequate description of the mass distribution within a DLA cluster also requires a continuum of scaling indices. Cases (ii) and (iii), which are characterized by two differently scaling lengths  $\bar{x}(\alpha)$  and  $\xi(\alpha, M)$  in the distribution  $N(\alpha, x, M)$ , display multiscaling features, while the single length scale case (i) does not show multiscaling.

The preceding discussion of multiscaling in DLA refers to ongoing work. The present results do not allow a final, unequivocal distinction among cases (i)–(iii). However, preliminary evidence supports case (iii) [14].

We note that the multiscaling of the density profile of the cluster is intricately related to the “multifractal” properties of the  $\{p_i\}$ , where multifractality means that the function  $f(\alpha)$  extends over a range of different  $\alpha$  values. In cases where the localization of  $\alpha$ -sites is described by two distinct length scales – as in the weak and strong localization cases – multifractality of the  $\{p_i\}$  leads to multiscaling of  $\rho_A(x, M)$ .

## 7. Summary

In summary, we have (i) one “firm” numerical result,  $\log p_{\min} \sim (\log M)^2$ , given by eq. (5). We have also (ii) an analytic argument that this behavior follows from a void-neck model of DLA structure in which there exist self-similar voids separated by necks whose width does not scale. We also have (iii) a plausibility argument that the tips of DLA grow together until they are separated by a distance which is typically a few pixels, as well as visual evidence supporting this picture, and (iv) some understanding of why 3D is different from 2D in terms of the inability of the necks in 3D to cut off a volume of space. There are many open questions, however. These include the question of the distribution of neck sizes [15], whether larger 3D clusters will show a phase transition [9], the connection of DLA structure to the lack of self-similarity recently reported by B.B. Mandelbrot [19], and the nature of the DLA “skeleton” [20].

## Acknowledgements

We are grateful to A. Bunde and H.E. Roman for collaboration on the key formative stages of this project in 2D (which are reviewed in ref. [18]), to P. Meakin for collaboration on the 3D extensions, and to A. Aharony, P. Alstrøm, A.-L. Barabási, R. Blumenfeld, T.C. Halsey, A.B. Harris, G. Huber, T. Nagatani, L. Pietronero, D. Stauffer, P. Trunfio, and T. Vicsek for helpful discussions and to NSF and KBN grant 1293/P3/93 for financial support.

## References

- [1] T.A. Witten and L. Sander, *Phys. Rev. Lett.* 47 (1981) 1400.
- [2] P. Meakin, in: *Phase Transitions and Critical Phenomena*, Vol. 12, C. Domb and J.L. Lebowitz, eds. (Academic, Orlando, 1988);  
J. Feder, *Fractals* (Pergamon, New York, 1988);  
H.E. Stanley and N. Ostrowsky, eds., *Random Fluctuations and Pattern Growth*:

- Experiments and Models (Kluwer Academic Publishers, Dordrecht, 1988);  
 T. Vicsek, *Fractal Growth Phenomena* (World, Singapore, 1989);  
 H.E. Stanley and N. Ostrowsky, eds., *Correlations and Connectivity: Geometric Aspects of Physics, Chemistry and Biology*, Proc. 1990 Cargèse NATO ASI, Series E: Applied Sciences, Vol. 188 (Kluwer, Dordrecht, 1990);  
 A. Bunde and S. Havlin, eds., *Fractals and Disordered Systems* (Springer, Heidelberg 1991);  
 H. Takayasu, *Fractals in the Physical Sciences* (Manchester Univ. Press, Manchester, 1990).
- [3] H. Fujikawa and M. Matsushita, *J. Phys. Soc. Jpn.* 58 (1989) 3875.  
 [4] F. Family, B.R. Masters and D.E. Platt, *Physica D* 38 (1989) 98;  
 C. Amitrano, A. Coniglio, P. Meakin and M. Zannetti, *Fractals* 1 (1993).  
 [5] F. Caserta, H.E. Stanley, W. Eldred, G. Daccord, R. Hausman and J. Nittmann, *Phys. Rev. Lett.* 64 (1990) 95;  
 H.E. Stanley, F. Caserta, W. Eldred, G. Daccord, R. Hausman and J. Nittmann, *Bull. Am. Phys. Soc.* 34 (1989) 716;  
 F. Caserta, R.E. Hausman, W.D. Eldred, H.E. Stanley and C. Kimmel, *Neurosci. Lett.* 136 (1992) 198;  
 F. Caserta, W.D. Eldred, E. Fernandez, R.E. Hausman, L.R. Stanford, S.V. Buldyrev, S. Schwarzer and H.E. Stanley, Determination of fractal dimension of physiologically characterized neurons in two and three dimensions, *J. Neurosci. Methods*, submitted.  
 [6] E. Guyon and H.E. Stanley, *Les Formes Fractales* (Palais de la Découverte, Paris, 1991); *Fractal Forms* (Elsevier, Amsterdam 1991) [English Translation];  
 D. Stauffer and H.E. Stanley, *From Newton to Mandelbrot: A Primer in Modern Theoretical Physics* (Springer, Heidelberg, 1990);  
 B.B. Mandelbrot and C.J.G. Evertsz, *Nature* 348 (1990) 143.  
 [7] L. Pietronero, A. Erzan and C.J.G. Evertsz, *Phys. Rev. Lett.* 61 (1988) 861;  
 L.A. Turkevich and H. Scher, *Phys. Rev. Lett.* 55 (1985) 1026;  
 A. Coniglio, in: *On Growth and Form: Fractal and Non-Fractal Patterns in Physics*, H.E. Stanley and N. Ostrowsky, eds. (Nijhoff, Dordrecht, 1985) p. 101;  
 G. Parisi and Y.C. Zhang, *J. Stat. Phys.* 41 (1985) 1;  
 Y. Hayakawa, S. Sato and M. Matsushita, *Phys. Rev. A* 36 (1987) 1963;  
 T.C. Halsey, *Phys. Rev. Lett.* 59 (1987) 2067.  
 [8] P. Meakin, H.E. Stanley, A. Coniglio and T.A. Witten, *Phys. Rev. A* 32 (1985) 2364;  
 T.C. Halsey, P. Meakin and I. Procaccia, *Phys. Rev. Lett.* 56 (1986) 854;  
 C. Amitrano, A. Coniglio and F. di Liberto, *Phys. Rev. Lett.* 57 (1986) 1016;  
 P. Meakin, A. Coniglio, H.E. Stanley and T.A. Witten, *Phys. Rev. A* 34 (1986) 3325.  
 [9] J. Lee and H.E. Stanley, *Phys. Rev. Lett.* 61 (1988) 2945;  
 J. Lee, P. Alstrøm and H.E. Stanley, *Phys. Rev. A* 39 (1989) 6545;  
 B. Fourcade and A.M.S. Tremblay, *Phys. Rev. Lett.* 64 (1990) 1842.  
 [10] R. Blumenfeld and A. Aharony, *Phys. Rev. Lett.* 62 (1989) 2977;  
 P. Trunfio and P. Alstrøm, *Phys. Rev. B* 41 (1990) 896;  
 B. Mandelbrot and C.J.G. Evertsz, *Physica A* 177 (1991) 386;  
 C.J.G. Evertsz, P.W. Jones and B.B. Mandelbrot, *J. Phys. A* 24 (1991) 1889;  
 B.B. Mandelbrot, *Physica A* 168 (1990) 95;  
 B.B. Mandelbrot, C.J.G. Evertsz and Y. Hayakawa, *Phys. Rev. A* 42 (1990) 4528;  
 C.J.G. Evertsz and B.B. Mandelbrot, *Physica A* 185 (1992) 77;  
 C.J.G. Evertsz and B.B. Mandelbrot, *J. Phys. A* 25 (1992) 1981;  
 C.J.G. Evertsz, B.B. Mandelbrot and L. Woog, *Phys. Rev. A* 45 (1992) 5798.  
 [11] A.B. Harris and M. Cohen, *Phys. Rev. A* 41 (1990) 971;  
 A.L. Barabási and T. Vicsek, *J. Phys. A* 23 (1990) L729;  
 R. Ball and R. Blumenfeld, *Phys. Rev. A* 44 (1991) 828.

- [12] S. Schwarzer, J. Lee, A. Bunde, S. Havlin, H.E. Roman and H.E. Stanley, *Phys. Rev. Lett.* 65 (1990) 603;  
S. Schwarzer, J. Lee, S. Havlin, H.E. Stanley, P. Meakin, *Phys. Rev. A* 43 (1991) 1134;  
M. Wolf, *Phys. Rev. A* 43 (1991) 5504; *Phys. Rev. A* 47 (1993) 1448.
- [13] J. Lee, S. Havlin, H.E. Stanley and J.E. Kiefer, *Phys. Rev. A* 42 (1990) 4832;  
J. Lee, S. Havlin and H.E. Stanley, *Phys. Rev. A* 45 (1992) 1035.
- [14] A. Coniglio and M. Zannetti, *Physica A* 163 (1990) 325;  
C. Amitrano, A. Coniglio, P. Meakin and M. Zannetti, *Phys. Rev. B* 44 (1991) 4974;  
P. Ossadnik, *Physica A* 195 (1993) 319;  
J. Lee, A. Coniglio, S. Schwarzer and H.E. Stanley, *Phys. Rev. E* 48 (1993) 1305.
- [15] S. Schwarzer, S. Havlin and H.E. Stanley, *Phys. Rev. E* 49 (1994) 1181.
- [16] S. Schwarzer, M. Wolf, S. Havlin, P. Meakin and H.E. Stanley, *Phys. Rev. A* 46 (1992) R3016;  
S. Schwarzer, S. Havlin and H.E. Stanley, *Physica A* 191 (1992) 117.
- [17] C. Amitrano, P. Meakin and H.E. Stanley, *Phys. Rev. A* 40 (1989) 1713.
- [18] H.E. Stanley, A. Bunde, S. Havlin, J. Lee, E. Roman and S. Schwarzer, *Physica A* 168 (1990) 23;  
S. Havlin, A. Bunde, E. Eisenberg, J. Lee, H.E. Roman, S. Schwarzer and H.E. Stanley, *Physica A* 194 (1993) 288.
- [19] B.B. Mandelbrot, *Physica A* 191 (1992) 95.
- [20] S. Schwarzer, P. Ossadnik, S. Havlin and H.E. Stanley, to be published;  
S. Schwarzer, Ph.D. Thesis, Boston University (1993)